CHAPTER 3: MATHEMATICAL MODELLING

The present chapter aims to provide an analytical model based on mechanics of flow forming. Upper bound solution has been used to developing a mathematical model for estimation of power and forces. The upper bound model has been used by several authors to solve different problems. [83][6], [30], [51], [52] This chapter is broadly divided into two parts. The first part proposes a generalized upper bound model developed for a generalized roller profile. The second part takes a special case of velocity field and develops the model

3.1 Generalized Upper Bound Method

A generalized upper bound method has been proposed. The upper bound model serves two function

i. It should provide flexibility to choose the deformation zone by varying the surfaces separating the undeformed zone and deformation zone. For this, the model uses the approach followed by Lambert and Kobayashi [84].

ii. To develop a generalized expression of flow lines which always satisfies the volume constancy

3.1.1 Generalized Kinetically Admissible Velocity

Let the profile of the roller be represented by equation (3.1) as function of z as

$$r = \emptyset_i(z) \tag{3.1}$$

Flow lines are the streamlines that are assumed to be represented by $\emptyset(z)$. Let the flow lines be given as

$$r = \emptyset_i(z) = \emptyset(z) + C_i \tag{3.2}$$

where C_i is constant .

$$C_i = \frac{C}{n} \tag{3.3}$$

where n is the number of flow lines in the deformation region.

Let the surfaces S_3 and S_1 are given as a function of z. Let surface 1 is represented by equation

$$r = \varphi_1(z) \tag{3.4}$$

Similarly, surface 3 is represented by equation

$$r = \varphi_3(z) \tag{3.5}$$

In the present model, the surface 1, given by $\varphi_1(z)$ generated by the intersection points of flow lines $\emptyset_i(z)$ and $z = z_i$ ($z_0 \leq z_i \leq z_n$) while surface 3, given by $\varphi_3(z)$ generated by the intersection points of flow lines $\emptyset_i(z)$ and $z = z_{n+i}$ $(z_n \leq z_{n+i} \leq z_e)$ a shown in Figure 3.1

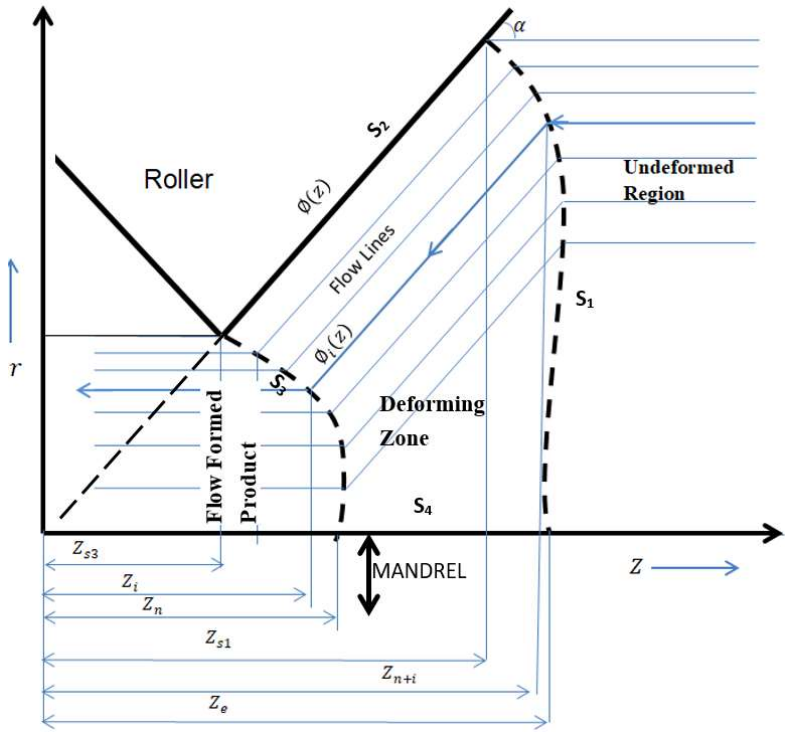

Figure 3.1: Schematic diagram for developing generalized upper bound mathematical model

Following assumptions are made for developing the mathematical model:

(i) The material in the zone I and III are treated as rigid.

(ii) The z coordinates of surface 3 can be varied as

$$z_i = z_{s3} + \frac{i-1}{n-1}(z_n - z_0) \tag{3.6}$$

Where n = number of flow lines and z_n is the intersection point of $\varphi_3(z)$ with r=0 line ie z intercept and z_i is the z coordinate of ith point on the surface 3.

(iii) The z coordinates of surface 1 can be varied as

$$z_{n+i} = z_{s1} + \frac{i-1}{n-1}(z_e - z_{s1}) \tag{3.7}$$

z_{s1} is intersection of $\varphi_1(z)$ with roller i.e. end point of roller section under consideration.

(iv) It has been assumed that $z_e = m' z_n$, where m' is a constant which can be varied to control the length of deformation zone in the model.

where m can range from

$$1 \leq m' \leq \left(\frac{(z_{s3} - z_{s1})}{z_n} + 1\right) \tag{3.8}$$

(v) The velocity is assumed to be only axial in zone I and zone III.

(vi) Plane strain condition is assumed in zone II and V_θ is assumed to zero.

The kinetically admissible velocity field should satisfy:

(a) Volume constancy criteria

$$\dot{\epsilon_{rr}} + \dot{\epsilon_{\theta\theta}} + \dot{\epsilon_{zz}} = 0 \tag{3.9}$$

(b) boundary conditions in zone I , that is

$$V_z = V_o \; ; V_\theta = 0; V_r = 0 \tag{3.10}$$

In Zone II ,

$$V_\theta = 0 \tag{3.11}$$

In Zone III,

$$V_z = V_f \; ; V_\theta = 0; V_r = 0 \tag{3.12}$$

3.2 Developing a generalized kinetically admissible velocity fields.

The flow lines in zone II was given by equation (3.2. Differentiating equation (3.2 with respect to time, we get

$$\frac{\partial r}{\partial t} = \frac{\partial \emptyset_i(z)}{\partial z}\frac{\partial z}{\partial t} \tag{3.13}$$

$$V_r = \emptyset'(z)V_z \tag{3.14}$$

The strain rates can be given as

$$\dot{\epsilon_{rr}} = \frac{\partial V_r}{\partial r} \tag{3.15}$$

$$\dot{\epsilon_{\theta\theta}} = \frac{\partial V_\theta}{r\partial\theta} + \frac{V_r}{r} \tag{3.16}$$

$$\dot{\epsilon_{zz}} = \frac{\partial V_z}{\partial z} \tag{3.17}$$

$$\dot{\epsilon_{r\theta}} = \frac{1}{2}\left(\frac{\partial V_\theta}{\partial r} + \frac{1}{r}\frac{\partial V_r}{\partial\theta} - \frac{V_\theta}{r}\right) \tag{3.18}$$

$$\dot{\epsilon_{\theta z}} = \frac{1}{2}\left(\frac{\partial V_\theta}{\partial z} + \frac{1}{r}\frac{\partial V_z}{\partial\theta}\right) \tag{3.19}$$

$$\dot{\epsilon_{zr}} = \frac{1}{2}\left(\frac{\partial V_r}{\partial z} + \frac{\partial V_z}{\partial r}\right) \tag{3.20}$$

The normal strain rate is given below. Equating the value of V_r in equation (3.15

$$\dot{\epsilon_{rr}} = \frac{\partial}{\partial r}(\emptyset'(z)V_z)$$

$$= V_z\,\emptyset''(z)\frac{\partial z}{\partial r} + \emptyset'(z)\frac{\partial V_z}{\partial z}\frac{\partial z}{\partial r} \tag{3.21}$$

Also, differentiating equation (3.2 with respect to z

$$\frac{\partial r}{\partial z} = \emptyset'(z) \tag{3.22}$$

Putting equation (3.22 in equation (3.21

$$\dot{\epsilon_{rr}} = V_z\,\emptyset''(z)\frac{1}{\emptyset'(z)} + \emptyset'(z)\frac{\partial V_z}{\partial z}\frac{1}{\emptyset'(z)} \tag{3.23}$$

Or,

$$\dot{\epsilon_{rr}} = V_z\,\emptyset''(z)\frac{1}{\emptyset'(z)} + \frac{\partial V_z}{\partial z} \tag{3.24}$$

Also

$$\dot{\epsilon_{\theta\theta}} = \frac{\partial V_\theta}{r\partial\theta} + \frac{V_r}{r}$$

$$= 0 + \frac{V_r}{r} = \frac{V_r}{r} \quad (3.25)$$

Putting equation (3.2 and (3.14 in (3.25

$$\dot{\epsilon_{\theta\theta}} = \frac{\emptyset'(z)V_z}{\emptyset(z)} \quad (3.26)$$

Putting the values of equations (3.17, (3.24, and (3.26 in equation (3.9, we get

$$V_z\,\emptyset''(z)\frac{1}{\emptyset'(z)} + \frac{\partial V_r}{\partial z} + \frac{\emptyset'(z)V_z}{\emptyset(z)} + \frac{\partial V_z}{\partial z} = 0 \quad (3.27)$$

Simplifying the above expression,

$$V_z\left(\emptyset''(z)\frac{1}{\emptyset'(z)} + \frac{\emptyset'(z)}{\emptyset(z)}\right) + 2V'_z = 0 \quad (3.28)$$

Rearranging,

$$\left(\emptyset''(z)\frac{1}{\emptyset'(z)} + \frac{\emptyset'(z)}{\emptyset(z)}\right) = -2\frac{V'_z}{V_z} \quad (3.29)$$

Integrating both sides, we get

$$\int\left(\emptyset''(z)\frac{1}{\emptyset'(z)} + \frac{\emptyset'(z)}{\emptyset(z)}\right)dz = \int -2\frac{V'_z}{V_z}dz \quad (3.30)$$

Solving,

$$\ln\emptyset'(z) + \ln\emptyset(z) = -2\ln V_z + \ln a^2 \quad (3.31)$$

Where a^2 is taken as constant of integration,

Simplifying equation (3.31

$$\ln\left(\emptyset(z)\emptyset'(z)\right) = 2\ln\left(\frac{a}{V_z}\right) \quad (3.32)$$

Simplifying again,

$$\emptyset(z)\emptyset'(z) = \left(\frac{a}{V_z}\right)^2 \quad (3.33)$$

Rearranging,

$$V_z = \frac{a}{\sqrt{\emptyset(z)\emptyset'(z)}} \quad (3.34)$$

Equation (3.34 gives the generalized kinetically admissible velocity in axial direction in terms of chosen flow lines. The velocity fields in zone II is therefore given as axial velocity, given by equation (3.34

Radial velocity in zone II can be obtained by substituting (3.34 in equation (3.14.

From equation (3.14 ; $V_r = \emptyset'(z)V_z$.

Therefore,

$$V_r = a\sqrt{\frac{\emptyset'(z)}{\emptyset(z)}} \quad (3.35)$$

And

$$V_\theta = 0 \quad (3.36)$$

3.3 Conditions on choice of suitable flow lines

The flow lines are chosen so that the curves are continuous and differentiable at all the points in the deformable zone. The only velocity discontinuity that should be present should be at the surfaces S_1, S_2. S_3 and S_4.

Some of the flow lines that can be

a) Linear flow lines :

Flow lines can be assumed to

$$r = \emptyset(z) = a_i z + b_i \quad (3.37)$$

where a_i and b_i are the constants

b) Polynomial flow lines of order n, which is given as

$$r = \emptyset(z) = \sum_{i=0}^{i=n} a_i z^i \quad (3.38)$$

where a_i is the coefficient of z^i

3.4 Upper bound formulation

Based on upper bound theory proposed by Prager and Hodge [85], for a rigid plastic von Mises material and amongst all kinematically admissible velocity fields, the velocity field should be chosen such that minimizes the actual maximum energy supplied J*, where

$$J^* = \frac{2}{\sqrt{3}}\sigma_0 \int_v \sqrt{\frac{1}{2}\dot{\epsilon}_{ij}\dot{\epsilon}_{ij}}dV + \int_s \tau|\Delta V|ds + \int_s mk|\Delta V|ds \quad (3.39)$$

In equation (3.39), the first term expresses power for internal deformation over the volume of the deforming body. The second term expresses shear power over surfaces of velocity discontinuities and the third term expresses the power loss due to friction at all surfaces in contact with work-piece.

3.4.1 Power for internal deformation over the volume of deforming body

Let power required for internal deformation be given as

$$J_1^* = \frac{2}{\sqrt{3}}\sigma_0 \int_v \sqrt{\frac{1}{2}\dot{\epsilon}_{ij}\dot{\epsilon}_{ij}}dV \quad (3.40)$$

The term $\frac{2}{\sqrt{3}}\sigma_0$ is called as effective stress while $\sqrt{\frac{1}{2}\dot{\epsilon}_{ij}\dot{\epsilon}_{ij}}$ is called as effective strain $\bar{\epsilon}$.

The effective strain in cylindrical coordinates is given as

$$\bar{\epsilon} = \sqrt{\frac{1}{2}\dot{\epsilon}_{ij}\dot{\epsilon}_{ij}} \quad (3.41)$$

$$= \frac{2}{3}\sqrt{\frac{1}{2}[(\dot{\epsilon}_{rr}-\dot{\epsilon}_{\theta\theta})^2 + (\dot{\epsilon}_{\theta\theta}-\dot{\epsilon}_{zz})^2 + (\dot{\epsilon}_{zz}-\dot{\epsilon}_{rr})^2] + 3\left(\dot{\epsilon}_{r\theta}{}^2 + \dot{\epsilon}_{\theta z}{}^2 + \dot{\epsilon}_{rz}{}^2\right)} \quad (3.42)$$

Simplifying, the above equation,

$$= \frac{\sqrt{2}}{3}\sqrt{\left[\dot{\epsilon}_{\theta\theta}{}^2 + \dot{\epsilon}_{rr}{}^2 + \dot{\epsilon}_{zz}{}^2 + 3\left(\dot{\epsilon}_{r\theta}{}^2 + \dot{\epsilon}_{\theta z}{}^2 + \dot{\epsilon}_{rz}{}^2\right)\right]} \quad (3.43)$$

The strain rates can be determined by choosing a suitable velocity field. Equation (3.34 to (3.36 provides the generalized velocity field as a function of z

$V_z = \frac{a}{\sqrt{\emptyset(z)\emptyset'(z)}}$, $V_r = a\sqrt{\frac{\emptyset'(z)}{\emptyset(z)}}$ and $V_\theta = 0$.

So,

$$\dot{\epsilon_{rr}} = \frac{\partial V_r}{\partial r} = \frac{\partial V_r}{\partial z}\frac{\partial z}{\partial r} \tag{3.44}$$

Using equation (3.1 and equation (3.44,

$$\dot{\epsilon_{rr}} = \frac{\partial}{\partial r}\left(a\sqrt{\frac{\emptyset'(z)}{\emptyset(z)}}\right)\frac{1}{\emptyset'(z)} \tag{3.45}$$

Solving,

$$\dot{\epsilon_{rr}} = \frac{a}{\emptyset'(z)}\left[-\frac{1}{2}\sqrt{\emptyset'(z)}\ \frac{\emptyset'(z)}{\emptyset(z)^{\frac{3}{2}}} + \frac{1}{2}\frac{1}{\sqrt{\emptyset(z)}}\frac{\emptyset''(z)}{\sqrt{\emptyset'(z)}}\right] \tag{3.46}$$

$$\dot{\epsilon_{rr}} = \frac{a}{2\sqrt{\emptyset(z)}}\left[\frac{\emptyset''(z)}{\emptyset'(z)^{\frac{3}{2}}} - \frac{\emptyset'(z)^{\frac{1}{2}}}{\emptyset(z)}\right] \tag{3.47}$$

Similarly, from the equation (3.16

$$\dot{\epsilon_{\theta\theta}} = \frac{\partial V_\theta}{r\partial\theta} + \frac{V_r}{r}$$

$$\dot{\epsilon_{\theta\theta}} = a\sqrt{\frac{\emptyset'(z)}{\emptyset(z)}}\ \frac{1}{\emptyset(z)} \tag{3.48}$$

Similarly, from the equation (3.17

$$\dot{\epsilon_{zz}} = \frac{\partial V_z}{\partial z}$$

$$\dot{\epsilon_{zz}} = -\frac{a}{2}\left[\frac{\emptyset'(z)^{\frac{1}{2}}}{\emptyset(z)^{\frac{3}{2}}} + \frac{\emptyset''(z)}{\emptyset(z)^{\frac{1}{2}}\emptyset'(z)^{\frac{3}{2}}}\right] \tag{3.49}$$

From equation (3.20, $\dot{\epsilon_{rz}}$ can be calculated as

$$\dot{\epsilon_{rz}} = \frac{1}{2}\left(\frac{\partial V_r}{\partial z} + \frac{\partial V_z}{\partial r}\right)$$

$$\dot{\epsilon_{rz}} = \frac{a}{4}\left[\left(\frac{\emptyset''(z)}{\emptyset(z)^{\frac{1}{2}}\emptyset'(z)^{\frac{1}{2}}} - \frac{\emptyset'(z)^{\frac{1}{2}}}{\emptyset(z)^{\frac{3}{2}}}\right) - \left(\frac{1}{\emptyset'(z)}\right)\left(\frac{\emptyset'(z)^{\frac{1}{2}}}{\emptyset(z)^{\frac{3}{2}}} + \frac{\emptyset''(z)}{\emptyset(z)^{\frac{1}{2}}\emptyset'(z)^{\frac{3}{2}}}\right)\right] \tag{3.50}$$

Rest all other strain rates are taken as zero, therefore

$$\dot{\epsilon_{r\theta}} = \dot{\epsilon}_{\theta z} = 0 \tag{3.51}$$

Equation (3.48 to (3.51 gives the generalized strain rates as a function of flow functions. For force estimation, the velocity field is assumed that should correspond to the contour of the tool given by $r = \emptyset(z)$. Once the $\emptyset(z)$ is chosen, all the velocity fields and strain rates are determined

In the present investigation, the profile of the tool is taken as linear. Hence, a linear relationship between r and z is assumed by assuming linear flow lines given by equation (3.52

Another assumption is taken that the surface bounding the deformation zone are taken as linear as shown in Figure 3.2. A linear relationship between r and z is assumed by assuming linear flow lines given by equation (3.52)

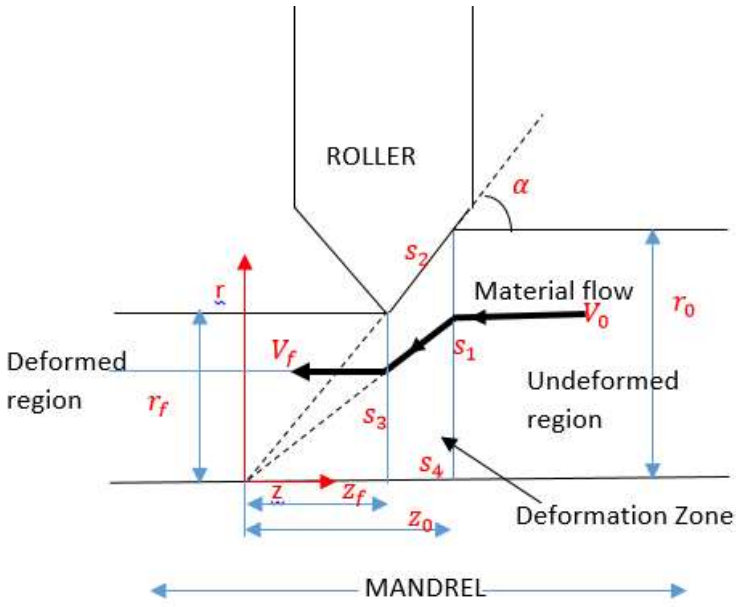

Figure 3.2: Schematic diagram showing Surface of discontinuities S_1, S_2, S_3 and S_4

Assuming,

$$r = \emptyset(z) = m\, z \tag{3.52}$$

Where m is slope of the curve between r and z

Also,

$$\frac{\partial r}{\partial z} = \emptyset'(z) = m; \text{ and } \emptyset''(z) = 0 \quad (3.53)$$

Putting equation (3.52 and equation (3.53 to obtain the velocity fields,

$$V_z = \frac{a}{\sqrt{(m\,z)m}}$$

Or,

$$V_z = \frac{a}{m\sqrt{z}} \quad (3.54)$$

Similarly,

$$V_r = a\sqrt{\frac{m}{m\,z}}$$

$$V_r = \frac{a}{\sqrt{z}} \quad (3.55)$$

$$V_\theta = 0 \quad (3.56)$$

The strain rates would be

$$\dot{\epsilon_{zz}} = -\frac{a}{2m}\frac{1}{Z^{3/2}} \quad (3.57)$$

$$\dot{\epsilon_{rr}} = -\frac{a}{2m}\frac{1}{Z^{3/2}} \quad (3.58)$$

And

$$\dot{\epsilon_{\theta\theta}} = \frac{a}{m}\frac{1}{Z^{3/2}} \quad (3.59)$$

$$\dot{\epsilon_{rz}} = \frac{1}{2}\left(\frac{\partial V_r}{\partial z} + \frac{\partial V_z}{\partial r}\right) \quad (3.60)$$

$$\dot{\epsilon_{rz}} = -\frac{a}{4}\left[\left(\frac{1}{(z)^{\frac{3}{2}}}\right)\left(1 - \frac{1}{m^2}\right)\right] \quad (3.61)$$

And, $\dot{\epsilon_{r\theta}} = \dot{\epsilon}_{\theta z} = 0$

The effective strain rate will be given as

$$\sqrt{\frac{1}{2}\dot{\epsilon}_{ij}\dot{\epsilon}_{ij}} = \frac{\sqrt{2}}{3}\sqrt{\left[\dot{\epsilon}_{\theta\theta}{}^2 + \dot{\epsilon}_{rr}{}^2 + \dot{\epsilon}_{zz}{}^2 + 3\left(\dot{\epsilon}_{r\theta}{}^2 + \dot{\epsilon}_{\theta z}{}^2 + \dot{\epsilon}_{rz}{}^2\right)\right]}$$

$$\bar{\epsilon}\cdot = \frac{\sqrt{2}}{3}\sqrt{\left[\dot{\epsilon}_{\theta\theta}{}^{\dot{2}} + \epsilon_{rr}{}^2 + \dot{\epsilon}_{zz}{}^2 + 3\left(\dot{\epsilon}_{rz}{}^2\right)\right]} \tag{3.62}$$

$$= \frac{\sqrt{2}}{3}\sqrt{\left[\frac{a^2}{m^2z^3} + \frac{1}{4}\frac{a^2}{m^2z^3} + \frac{1}{4}\frac{a^2}{m^2z^3} + \frac{3}{16}\left(\frac{a^2}{(z)^3}\right)\left(1 - \frac{1}{m^2}\right)^2\right]} \tag{3.63}$$

$$= \frac{\sqrt{2}}{3}\sqrt{\left[\frac{3a^2}{2m^2z^3} + \frac{3}{16}\left(\frac{a^2}{(z)^3}\right)\left(1 - \frac{1}{m^2}\right)^2\right]} \tag{3.64}$$

Simplifying,

$$\bar{\epsilon}\cdot = \frac{1}{\sqrt{24}}\frac{a}{mz^{3/2}}\sqrt{\left[\left(8 + \left(m - \frac{1}{m}\right)^2\right)\right]} \tag{3.65}$$

The effective strain rate comes out to be a function of slope m

$$\bar{\epsilon}\cdot = S(m)\frac{1}{(z)^{3/2}} \tag{3.66}$$

Where $S(m)$ denotes the function of m which is independent of z

And,

$$S(m) = \frac{1}{\sqrt{24}}\frac{a}{m}\sqrt{\left(8 + \left(m - \frac{1}{m}\right)^2\right)} \tag{3.67}$$

From equation (3.40 ,

$$J_1^* = \frac{2}{\sqrt{3}}\sigma_0\int_v \sqrt{\frac{1}{2}\dot{\epsilon}_{ij}\dot{\epsilon}_{ij}}dV$$

$$= \frac{2}{\sqrt{3}}\sigma_0\int_v S(m)\frac{1}{(z)^{3/2}}dV \tag{3.68}$$

To calculate the volume, the contact area is calculated on the basis of Figure 3.3 where R_m is radius of mandrel and β is the angle subtended by contact zone at the centre of the mandrel.

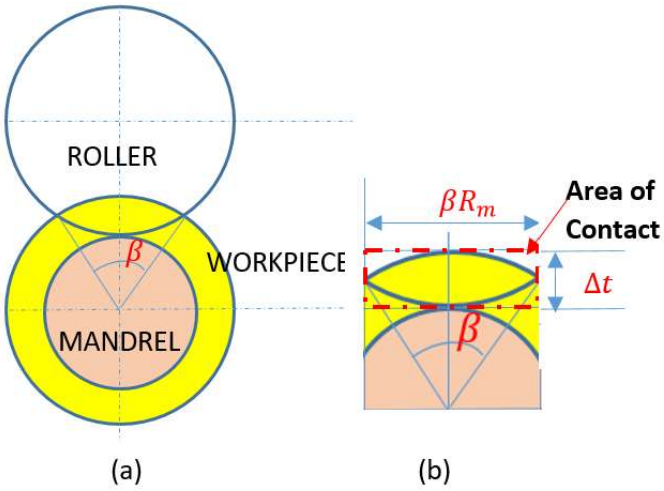

Figure 3.3: (a) Schematic diagram representing front view showing interaction zone between the roller and the workpiece (b) contact area taken in investigation

Let,

$$b = \beta R_m \tag{3.69}$$

$dV = bdA = brdz = b(m\,z)dz$

Therefore,

$J_1^* = \frac{2}{\sqrt{3}}\sigma_0 \int_v S(m) \frac{1}{(z)^{3/2}} dV$

$= \left| \frac{2}{\sqrt{3}}\sigma_0 S(m) \int_v \frac{1}{(z)^{3/2}} brdz \right|$

$= \left| \frac{2}{\sqrt{3}}\sigma_0 S(m) \int_v \frac{1}{(z)^{3/2}} b(m\,z)dz \right|$

$= \left| \frac{2}{\sqrt{3}}\sigma_0 mS(m) \int_{z_0}^{z_1} \frac{1}{(z)^{1/2}} bdz \right|$

$= \left| \frac{2}{\sqrt{3}}\sigma_0 mS(m) b2(z)^{1/2} \Big|_{z_o}^{z_f} \right|$

$$= \left| \frac{4}{\sqrt{3}}\sigma_0 mS(m) b \left((z_0)^{1/2} - (z_f)^{1/2} \right) \right| \tag{3.70}$$

$= \left| \frac{4}{\sqrt{3}}\sigma_0 mS(m) b \left((z_0)^{1/2} - (z_f)^{1/2} \right) \right|$

Putting $z_0 = {}^{r_0}/_{m}$ and $z_i = {}^{r_i}/_{m}$

$$J_1^* = \frac{4}{\sqrt{3}}\sigma_0 m S(m) b\left(\left({}^{r_0}/_{m}\right)^{1/2} - \left({}^{r_f}/_{m}\right)^{1/2}\right)$$

$$J_1^* = \frac{4}{\sqrt{3}}\sigma_0\sqrt{m}\,S(m) b\left((r_0)^{1/2} - (r_i)^{1/2}\right) \quad (3.71)$$

3.4.2 Power loss due to velocity discontinuity

Power loss due to shear at the regions of velocity discontinuity can be given by

$$P_{vd} = \int_s \tau\,|\Delta Vs|ds \quad (3.72)$$

Using von- Mises yield criterion, the shear stress can be assumed as

$$\tau = K \quad (3.73)$$

Velocity discontinuity takes place at surface marked as S_1 to S_4 in Figure 3.2. Power loss associated with velocity discontinuity associated with surface S_1 would be

$$P_{vd_1} = \int_{s1} K\,|\Delta V_1|ds_1 \quad (3.74)$$

Where ds_1 = length of surface

$$= \int_0^{\alpha} K\,(V\sin\theta - 0)\,r_0 d\theta$$

As the steady state was assumed, the velocity flow perpendicular to the surface would not change. Therefore,

$$V\cos\theta = V_0 \quad (3.75)$$

$$P_{vd_1} = \int_0^{\alpha} K\,(V_0\tan\theta)\,r_0 d\theta \quad (3.76)$$

Or, $$P_{vd_1} = K\,V_0 r_0 \ln sec\,(\alpha) \quad (3.77)$$

Power loss associated with velocity discontinuity associated with surface S_2 would be

$$P_{vd_2} = \int_{s_2} K\,|\Delta V_2|ds \quad (3.78)$$

$$P_{vd_2} = \int_{s_2} K\,|\Delta V_2|ds$$

$$= \int_{r_o}^{r_f} K\,(V - V_0\,\cos\alpha)\frac{\Delta t}{\sin\alpha}dr \quad (3.79)$$

Since,

$$V = \sqrt{V_r^2 + V_z^2} \tag{3.80}$$

Therefore, equating values of V_z and V_r in terms of r, we get

$$V = \frac{a}{\sqrt{r}} \sqrt{m} \left(\frac{1}{m^2} + 1\right) \tag{3.81}$$

Equating (3.81 in (3.79 and solving

$$P_{vd_2} = K \frac{\Delta t}{\sin \alpha} \left(\frac{2a}{m^{3/2}} (1 + m^2)\left(\sqrt{r_0} - \sqrt{r_f}\right) - V_0 \cos \alpha \ \left(r_0 - r_f\right)\right) \tag{3.82}$$

Power loss associated with velocity discontinuity associated with surface S_3 would be

$$P_{vd_3} = \int_{s_3} K \ |\Delta V_3| ds \tag{3.83}$$

$$P_{vd_3} = \int_{s_3} K \ V sin \ \theta \ \ ds_3 \tag{3.84}$$

Or,

$$P_{vd_3} = \ Ka\sqrt{m}\sqrt{r_f} \left(\frac{1}{m^2} + 1\right) r_f (1 - \cos \alpha) \tag{3.85}$$

Therefore, total power loss due to velocity discontinuity at surface S_4 is taken as zero as there is no surface at which change in velocity takes place.

$$P_{vd} = P_{vd_1} + P_{vd_2} + P_{vd_3} \tag{3.86}$$

Where the values of P_{vd_1}, P_{vd_2} *and* P_{vd_3} are obtained from the (3.77, (3.82 and (3.85 respectively.

3.4.3 **Power loss due to friction**

The power loss due to friction takes place at two contact surfaces- between the workpiece and the roller surface and between the workpiece and the mandrel. The expression of power loss due to friction can be given by equation (3.87

$$P_{fric} = \int_s mk|\Delta V_s| dA \tag{3.87}$$

3.4.4 Power loss at work piece- roller contact region

The roller-workpiece contact region is a complex region and its area is dependent on the thickness reduction. To calculate the contact area between the rollers – workpiece, either the contact area can be approximated as

(i) a rectangle with surface area equals $\beta R_m \Delta t$ (refer Figure 3.3)

(ii) as an ellipse as shown in Figure 3.4. The major axis, 2a, of the above ellipse is equal to the chord of contact which can be given as

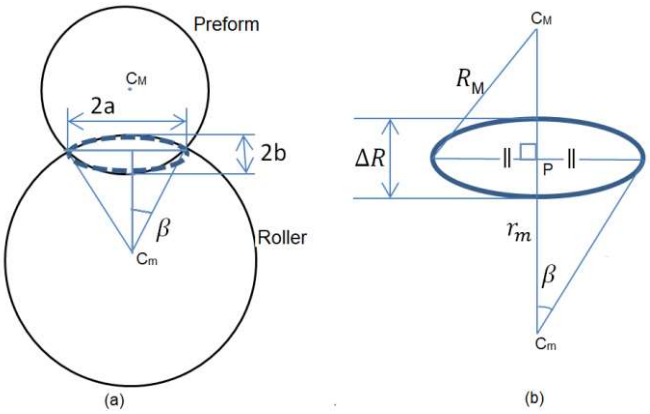

Figure 3.4: Roller – Workpiece contact region approximated as ellipse.

Area of contact (assumed to be an ellipse) is derived below.

Let. the major axis of the elliptical regions is $2a'$ and the minor axis is taken as $2b'$.

$$a' = r_m \sin\beta \tag{3.88}$$

$$= \sqrt{{R_M}^2 - (R_M - \frac{\Delta t}{2})^2} \tag{3.89}$$

Where,

$$\Delta R = \text{thickness reduction} = \Delta t = \text{final thickness} - \text{intial thickness} \tag{3.90}$$

And minor axis

$$b' = \frac{\Delta t}{2} = \xi \tag{3.91}$$

Therefore,

$$\text{The area of contact} = \pi ab \tag{3.92}$$

$$\text{Total frictional Area} = \pi \frac{\Delta t}{2} \sqrt{\frac{\Delta R^2}{4} + R_M \Delta t} \tag{3.93}$$

$$= \pi \frac{\Delta t}{2} \sqrt{R_M \Delta t} \text{ (assuming } \frac{\Delta R^2}{4} \ll R_M \Delta t) \tag{3.94}$$

Therefore, the total interaction area between tool and workpiece in the deformation zone (region 2) would be

$$A_{Tw} = \pi \frac{\Delta t}{2} \sqrt{R_M \Delta t} \tag{3.95}$$

$$P_{fric,TW} = \int_{s2} m_1 K V_0 \sin\alpha \, dA_{TW} \tag{3.96}$$

$$= m_1 k V_0 \sin\alpha \, \pi \frac{\Delta t}{2} \sqrt{R_M \Delta t} \tag{3.97}$$

3.4.5 **Power loss at workpiece- mandrel contact region**

Let the coefficient of friction between the mandrel and workpiece by m_2 .

Power loss due to friction at workpiece – mandrel interface will be

$$P_{fric,mw} = \int_{s4} m_2 K V_0 dA_{mw} = m_2 K V_0 (r_0 - r_f) \frac{\beta}{\pi} r_M \tag{3.98}$$

Where 2 Therefore, the total power P_T required for the deformation would be

$$P_T = P_{in} + P_{vd} + P_{fric} \tag{3.99}$$

The total power given by equation (3.99) doesn't include redundant work. So, the power calculated will be less than expected. To account for a factor η_a is introduced to take into account the redundant power and other losses during the experimentation. So the total power will be given by equation

$$P_{total} = \frac{P_T}{\eta_a} \tag{3.100}$$

3.5 Calculation of average force

The axial force F_a can be obtained from the power,

$$F_{axial} = \frac{P_{total}}{V_0} \tag{3.101}$$

Assuming circumferential force to be negligible in case of axisymmetric workpiece, the radial force F_r can be obtained using the equation (3.102)

$$F_r = \frac{F_a}{\tan\alpha} \tag{3.102}$$

The equation 3-101 gives an approximate relationship assuming the circumferential force to be zero. However, from the literature, the circumferential force would be least among the components of forces. Assuming, a finite value of circumferential force, then the radial force is obtained by modifying equation (3.102) by introducing another constant term η_r . The constant η_r is introduced to take care of the errors introduced due to neglecting of circumferential forces. The modified expression is given by (3.103)

$$F_{radial} = {}^{F_r}/_{\eta_r} \tag{3.103}$$

The net flow forming force can then be calculated as

$$F_{total} = \sqrt{{F_{radial}}^2 + {F_{axial}}^2} \tag{3.104}$$

Where F_{total} represents net flow forming forces.

The values of the constants η_a and η_r are always less than one. The values of these constants would depends on the material, the experimental conditions and also on the choice of velocity field function which is assumed to be linear in the present investigation. Hence, these constants must be calculated based on experimental data. In the present investigation, the values of η_a and η_r for Al6101 from initial trial.

3.5.1 Validation of Mathemtical model for Al6101 T6

3.5.1.1 Calculation of values of constants η_a and η_r for Al6101 T6

For Al6101, the results of FF02 are taken as reference for obtaining the values. For FF02, the following values are different variables are taken, mandrel radius = 63 mm, initial thickness =2.5mm, attack angle =30º, friction coefficient m1 and m2= 0.3 mm, feed =0.04mm /rev, mandrel RPM= 420 rpm and σ_0 = 280 MPa.

Table 3.1: Calculating value of $\boldsymbol{\eta_a}$ and $\boldsymbol{\eta_r}$ for Al6101 T6

Pass	%TR Per Pass	Calculated Axial force (N)	Experimental force (N)	η_a	Calculated Radial force (N)	Experimental radial force (N)	η_r
1	10	180.9	661.8	0.28	1114.4	1148.2	0.97
2	11.1	180.1	654.2	0.27	1133.5	1143.1	0.99
3	25	506.2	1580	0.32	2738.3	2813.2	0.97
4	16.7	178.9	673.2	0.26	1166.7	1186.9	0.98
5	20	179.24	705.3	0.25	1222.4	1251.2	0.97

From the experimental trial, the average value of η_a can be taken as 0.28 whereas η_r can be taken as 0.98. The low values of the constant suggest a complex state of stress. Using the values of η_a and η_r, the force model can be validated with the results of another experimental trial . The values of forces and the error of difference in measured force and the calculated force for the sample FF01 are summarised in Table 3.2.

Table 3.2: Validation of mathematical model for Al6101 T6

Pass	Δt (per pass mm)	Fa (cal) (N)	Fa (exp) (N)	% Error	Fr (cal) (N)	Fr(exp) (N)	Error (N)
1	0.1	646.0	665.3	2.99	1142.5	1114.5	2.45
2	0.2	1791.5	1695.8	5.34	3168.3	2939.0	7.24
3	0.2	1807.9	1887.9	4.43	3197.2	3271.9	2.34
4	0.2	1828.1	1985.7	8.62	3232.9	3441.4	6.45
5	0.1	657.1	702.6	6.9	1162.0	1217.7	4.79

From the table 3.2 , the difference between the experimental force and the calculated force from the model has been found to be less than 10% which validates the model proposed above for Al6101 material. The values of η_a for Al6101 in general would range from 0.25 to 0.35 while η_r would in general range from 0.95 to 0.99, depending on the geometrical and other process parameters. The η_r values are expected to close to 1 if circumferential forces magnitude becomes negligible.

3.5.2 Validation of the mathematical model for 7075

3.5.2.1 Calculation of values of constants η_a and η_r for Al7075

For Al7075, the results of 7F03 are taken as a reference for obtaining the values. The material is softened by heating the preform at 470ºC for 3 hours. The following values are different variables are taken, mandrel radius = 32.4 mm, initial thickness =1.5mm, attack

angle =30º, friction coefficient m1 and m2= 0.3 mm, feed =0.04mm /rev, mandrel RPM= 420 rpm and $\boldsymbol{\sigma_0}$ = 231.4 MPa. For calculation of the $\boldsymbol{\eta_a}$ and$\boldsymbol{\eta_r}$, the force values of experiments with Al7075 heat treated samples – sample 1(F04N250), sample 2 (F08N250), 7F02 and are validated with results of flow forming of samples 7F04 (Figure 4.25).

Table 3.3: Calculating value of $\boldsymbol{\eta_a}$ and $\boldsymbol{\eta_r}$ for heat treated samples of Al7075

Sample	%TR Per Pass	Calculated Axial force (N)	Experimental force (N)	η_a	Calculated Radial force (N)	Experimental radial force (N)	η_r
F04N250	33.3	478.4	1417.4	0.34	2749.4	2836.3	0.97
F08N250	33.3	478.4	1552.9	0.31	2749.4	2901.7	0.95
7F04	20	209.0	783.2	0.27	1201.1	1245.3	0.96
F04N420	33.3	478.4	1526.9	0.31	2749.4	2843	0.97
F08N420	33.3	478.4	1710.1	0.28	2749.4	2925.2	0.94

The result of the table shows that the consistency of the values of η_a and η_r in five different samples validates the mathematical model that have been proposed. The table shows the value of η_a lies between 0.27-0.32 and η_r lies between 0.94 - 0.97. The maximum error that can be introduced in axial force is given by

$$Maximum\ error\ in\ case\ of\ overestimation\ of\ axial\ force = \frac{(0.32-0.27)}{0.27} X100 = 19 \quad (3.105)$$

$$Maximum\ error\ in\ case\ of\ underestimation\ of\ axial\ force = \frac{(0.32-0.27)}{0.32} X100 = 16 \quad (3.106)$$

The maximum error is the case of maximum overestimation or underestimation. The error can be reduced by taking the average values of η_a =0.3, which mathematically reduces the maximum error in case of overestimation of axial force to 11% and in case of underestimation of axial force to be 6 %.

Similarly, the maximum error in radial force in case of overestimation would be given by equation ((3.106).

$$Maximum\ error\ in\ case\ of\ overestimation\ of\ radial\ force = \frac{(0.97 - 0.94)}{0.94} X100 = 3.2\% \quad (3.107)$$

$$Maximum\ error\ in\ case\ of\ underestimation\ of\ radial\ force = \frac{(0.97 - 0.94)}{0.97} X100 = 3.1\% \quad (3.108)$$

Therefore, a theoretical maximum error of 3.2% would be expected between the predicted radial forces and the experimental radial force. As the radial force is the dominant force, the low error values in radial force would converge the total error in estimation.

To check the validity of the model in multipass force estimation, the average value of η_a for Al7075 heat treated samples was taken as 0.3 and that of η_r is taken as 0.96. Taking the above values of η_a and η_r, the calculated force and experimental force for sample 7F04 are compared and the error in force is calculated . The results are shown in table 3.4.

Table 3.4: Validation of mathematical model using η_a =0.3 a nd η_r =0.96 for 7075 heat treated 7F04 (Figure 4.25)

Pass	%TR	Fa (cal) (N)	Fa (exp) (N)	| % Error |	Fr (cal) (N)	Fr(exp) (N)	|% Error|
1	26.67	1101.3	982.30	9.08	1967.8	1779.4	10.5
2	36.36	1124.3	1182.90	5.21	2008.9	1996.1	1.7
3	28.6	1072	1153.20	7.02	1746.2	1759.2	0.91

The result shown in the table shows the error in predicted values of axial force was within 10%. In the first two passes, the estimated force was found to be higher than the experimental force with the maximum in the above case was found to be 9.08%. In the third pass the calculated force was less than 7.02 % less than the experimental force. However the difference in calculated force and the experimental force was found to be 0.91% to 10.5 %. The result showed that the estimated force by the model was higher than experimental force for the first pass. The results showed that the mathematical model gave overestimation for initial passes but the mathematical model gave underestimation as the number of passes increases. The model therefore gave satisfactory result in the present investigation for the initial passes, however the result for multipass may vary if number of passes increases. Therefore, the model would be applicable for lower number of passes.

3.5.3 Validation of the mathematical model for Al2014

3.5.3.1 Calculation of values of constants ηa and ηr for Al2014

The preform of the Al2014 has been softened by heating the preform at 413ºC for 2 hours. The following values are different variables are taken, mandrel radius = 32.4 mm, initial

thickness =1.5mm, attack angle =30º, friction coefficient m1 and m2= 0.3 mm, feed =0.04mm /rev 0.08mm/rev mandrel RPM= 240 rpm and 420 rpm and σ_0 = 276.6 MPa.

The mathematical model suffers with the limitation that the contribution of the mandrel rpm and feed rate cancelled out. The variation of the flow forming forces with mandrel speed and the feed rates have not been accounted. The actual measurement of forces for samples F04N240, F08N240, F04N420, F08N420 (Figure 4.47) showed that the flow forming depends on the mandrel speed and feed.

As seen from section 3.5.2, the model would be more applicable for lower number of passes. The validity of the mathematical model has been checked for Al2014 have been checked for the second passes of the samples. Table 3.5 shows the values of $\boldsymbol{\eta_a}$ and $\boldsymbol{\eta_r}$ in the experiment study of Al2014.

Table 3.5: Calculation of mathematical model using $\boldsymbol{\eta_a}$ and $\boldsymbol{\eta_r}$ for 2014 heat treated samples.

Sample	%TR	Fa (cal) (N)	Fa (exp) (N)	$\boldsymbol{\eta_a}$	Fr (cal) (N)	Fr(exp) (N)	$\boldsymbol{\eta_r}$
2014(3)	20	133.2	452	0.29	230.9	798	0.29
2014(4)	30	251.80	698.2	0.36	436.5	1229.1	0.36
2014(5)	40	407.1	1067.3	0.38	705.6	1962.3	0.36

In the present investigation, the values of $\boldsymbol{\eta_a}$ and $\boldsymbol{\eta_r}$ for 2014 samples were found to be different than the values for Al6101 and Al7075. The value of $\boldsymbol{\eta_a}$ has been found to lie between 0.29 and 0.38 while the values of $\boldsymbol{\eta_r}$ has been found to vary between 0.29 and 0.36. The small variation in $\boldsymbol{\eta_a}$ and $\boldsymbol{\eta_r}$ validate the model with the experimental results.